❒   1

Modeling and Simulation of a Carrier-based PWM Voltage Source Inverter for a Nine Phase Induction Machine Drive

Omonowo David Momoh
Department of Computer, Electrical and Information Technology, Indiana University-Purdue University (IPFW)
Fort Wayne, Indiana, United States

Article Info	ABSTRACT
	The analysis of a carrier-based PWM two level voltage source inverter for a nine phase induction machine drive system is presented in this paper. Methods for generating zero-sequence signals during balanced and unbalanced condition are established. Simulation results for the analysis are presented. Two fault conditions involving the voltage source inverter and the nine-phase squirrel cage induction machine load are investigated. For the two fault scenarios considered, the effects on the performance characteristics of the induction machine load are highlighted. The simulation results obtained show that the two imbalance conditions considered result in substantial oscillations on the electromagnetic torque of the machine with attendant reduction in the torque rating. There is also large slip in the rotor speed.

Corresponding Author:

Omonowo David Momoh
Department of Computer, Electrical and Information Technology
Indiana University-Purdue University (IPFW)
Fort Wayn, Indiana, United States
Email: momohd@ipfw.edu

1. INTRODUCTION

Multiphase machines are electrical generators or motors with the number of phases greater than three (n > 3). When compared to three phase machines, multiphase machines have greater degrees of freedom which has enabled some improvements in the system's performance [1]-[5]. The advantages of multiphase machine over their three phase counterparts are well documented in [6]-[12]. They include: higher reliability and increased power density, enhanced fault tolerant capability, extended speed/torque capability, reduced amplitude/increased frequency of pulsating torque, reduced rotor harmonic currents, and reduced current per phase without increasing the voltage per phase. Also, in multiphase machine, extra-torque can be produced from the interactions of current and spatial harmonics of the same order. For instance, in nine phase machine, the third, fifth, and seventh harmonics can be harnessed to generate average torque which adds up to the torque produced by the fundamental current component.

At the core of a multiphase machine drive is the power electronics technology. The advancement in power electronics technology has made it possible to produce any number of phases using a DC/AC voltage source inverter (VSI). Carrier-based sinusoidal pulse-width modulation (SPWM) is the most popular and widely used PWM technique. This is because of the simple implementation in both analog and digital realizations when compared to the space-vector PWM (SVPWM), which is found to be more intense from computational and complexity viewpoints [13], [15]. Carrier-based SPWM also known as the comparison pulse-width modulator compares a high-frequency triangular (double edge) or saw-tooth (single-edge) carrier with reference signals (modulation signals) thereby creating gating pulses for the switches in the power circuit [15], [16].

The neutral point of most ac motor drive and utility interface applications is isolated and

consequently, there is no neutral current path. The absence of the neutral current path in the load provides a degree of freedom in determining the duty cycle of the inverter switches [17]. The difference in potential between the load neutral point ('n') and the center point of the dc-link capacitor ('o') of the VSI is called the zero-sequence voltage, v_{no}. The zero-sequence voltage can take any value which can be subsequently injected into the modulation signals to achieve any of the following desirable properties: reduced switching losses, improved waveform quality, and increased linear modulation range [3]. If the injected zero-sequence signal is continuous, it produces a continuous PWM (CPWM) scheme; however, when it is discontinuous with the potential for the modulator to have phase segments clamped to the positive or negative dc rails, the modulation scheme is called discontinuous PWM (DPWM). In DPWM, there is no switching (and consequently no switching losses) in those intervals when there is discontinuous modulation. A carrier based PWM method comprising of all DPWM schemes is called the generalized discontinuous PWM (GDPWM) [13], [18].

Much ground has been covered on PWM schemes for a multiphase VSI using either carrier-based PWM or SVPWM technique. The goal of this paper is to implement a thorough simulation and analysis of a carrier-based SPWM voltage source inverter for a nine-phase induction machine drive. This is done through modeling and simulation of the drive system. In so doing, the work proposed in [3] is extended to a nine-phase system. Also, beyond the work done for five-phase VSI drive system in [3] and [15], plots showing the performance characteristics of the nine-phase induction machine are presented in this paper. Figure 1 is a simplified schematic diagram of a two-level converter (VSI) supplying a nine-phase squirrel cage induction machine.
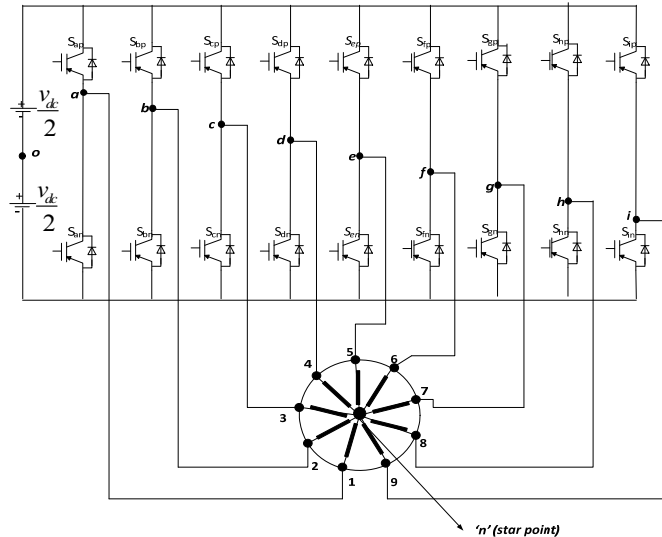

Figure 1. Two-level nine-phase VSI supplying a nine-phase squirrel cage induction machine

2. MODELING OF CONTINUOUS CARRIER-BASED PWM FOR NINE PHASE

The principles of carrier-based PWM for a three-phase VSI are also applicable to a multiphase VSI [13]. Consequently, the load voltage equations for the nine-phase VSI supplying nine-phase squirrel cage induction machine as depicted in Figure 1 are given as follows:

$$v_{jn} = L_{js} p i_{js} + r_{js} i_{js} \tag{1}$$

v_{jn} are the phase to neutral output voltage from the VSI, i_{js} are the phase currents from the VSI to the load, L_{js} are the induction machine stator inductances, r_{js} are the induction machine stator resistances, p is a differential operator (d/dt), $j = a, b, c, d, e, f, g, h, i$.

The turn-on and turn-off of the switching devices for the nine-phase VSI shown in Figure 1 are represented by an existence function. The existence function has a value of unity and zero when the switching device is turned on and turned off respectively. In its simplest form, an existence function of a two-

level converter can be represented as S_{jk}, $j = a, b, c, d, e, f, g, h, i$ and $k = p, n$. j depicts the load phase to which the switching device is connected and k represents the top (p) and bottom (n) device of an inverter leg. Consequently, from Figure 1, S_{ap} and S_{an} take a value of zero or unity and the two constitute the existence function of the top device and bottom device of the inverter leg connected to phase 'a' of the nine phase induction machine load [3], [13].

There are $2^9 = 512$ switching possibilities (arrangements) during the operation of a nine-phase VSI. The operation of a carrier-based PWM can be divided into two modes-linear modulation mode and nonlinear modulation mode. Under the linear modulation mode, the peak of a modulation signal is less than or equal to the peak of the carrier signal and consequently the gain is approximately unity. However, when the peak of a modulation signal is greater than the peak of the carrier signal, over-modulation occurs and the gain is generally less than unity. For operation in the linear modulation region, modulation is defined as the ratio of the fundamental component amplitude of the line-to-neutral (phase) inverter output voltage to one-half of the DC bus voltage [3], [19]. This is given as:

$$M_j = \frac{V_j}{0.5 V_{dc}} \tag{2}$$

Where M_j is the modulation index (magnitude of the modulation), V_j is the magnitude of the fundamental inverter output voltage, and V_{dc} is the magnitude of the dc bus voltage.

The voltage between the jth inverter phase and the center point of the dc-link capacitor ('o') otherwise known as pole (switched) inverter phase voltage, v_{jo}, is related to the load phase voltage, v_{jn}, as follows:

$$v_{jo} = v_{jn} + v_{no} \tag{3}$$

Where v_{no} is the common-node zero-sequence voltage as defined in section I above. The constraint imposed by Kirchhoff's Voltage Law (*KVL*) on the two switches in an inverter leg is such that the existence functions for the top and bottom devices must be complimentary of each other. This is expressed in (4).

$$S_{jp} + S_{jn} = 1 \tag{4}$$

Violating this constraint will cause the short circuiting of the dc bus voltage. However, for absolute control of currents and output voltages, one device in each leg must be turned on at all operating tines. There is a relationship between the switched voltage, the existence functions, and the dc bus voltage given as follows:

$$v_{jo} = \frac{1}{2} v_{dc} \left(S_{jp} - S_{jn} \right) \tag{5}$$

From (4),

$$S_{jn} = 1 - S_{jp} \tag{6}$$

The complimentary property of S_{jp} and S_{jn} can be further expressed as:

$$\begin{aligned} S_{jp} &= \overline{S}_{jn} \\ S_{jn} &= \overline{S}_{jp} \end{aligned} \tag{7}$$

By substituting (6) into (5), we have:

$$v_{jo} = \frac{1}{2} v_{dc} \left(2 S_{jp} - 1 \right) \tag{8}$$

The nine switched voltages expressed in (3) can be summed up as follows:

$$\sum_{j=a}^{i} v_{jo} = \sum_{j=a}^{i} v_{jn} + 9 v_{no} \qquad (9)$$

A symmetrical induction machine in a normal operation condition represents a balanced star-connected load. Consequently, the sum of the phase currents equal to zero. Thus:

$$\sum_{j=a}^{i} i_{js} = 0 \qquad (10)$$

Substituting (10) into (1) implies that the sum of the inverter phase-to-neutral output voltage (load voltage) equals to zero as shown in (11).

$$\sum_{j=a}^{i} v_{jn} = 0 \qquad (11)$$

By taking into consideration Equation (10) and (11), the common-node zero-sequence voltage can be expressed in terms of the switched voltage as follows:

$$v_{no} = \frac{1}{9} \sum_{j=a}^{i} v_{jo} \qquad (12)$$

Also, by substituting (8) into (12), the zero-sequence voltage can be expressed in terms of the existence function and the dc bus voltage as given in (13).

$$v_{no} = \frac{v_{dc}}{9} \left[\sum_{j=a}^{i} S_{jp} - \frac{9}{2} \right] \qquad (13)$$

By substituting (13) and (8) into (3), the inverter phase-to-neutral voltage is expressed in terms of the existence functions and dc bus voltage as follows:

$$v_{jn} = \frac{v_{dc}}{9} \left(8 S_{jp} - \sum_{\substack{q=a \\ q \ne j}}^{i} S_{qp} \right), \qquad (14)$$

$$q, j = a, b, c, d, e, f, g, h, i$$

2.1. Nineth-Harmonic Injection

It has been proposed that the injection of the nth-harmonic into the reference modulation signals of an *n-phase* system effectively increases the linear modulation range without moving into over-modulation region [20], [21]. This technique has led to higher output fundamental voltage than using simple sinusoidal carrier based PWM [3], [15]. The optimal level of the nth-harmonic component is found to be:

$$v_n = \pm v_j \frac{\sin(\pi/2n)}{n} \qquad (15)$$

Equation (15) takes a positive sign for n = 3, 7, 11, 15,…., and negative sign for n = 5, 9, 13, 17, ……. Thus, for a nine-phase system, the injected nineth harmonic is negative and the resulting zero-sequence signal is given as:

$$v_{no9}(t) = \left(-v_j \frac{\sin(\pi/18)}{9} \right) \sin(9\omega t) \qquad (16)$$

The maximum possible modulation index in the linear region in the case of the nth harmonic injection has been derived to be:

$$M = \frac{1}{\cos(\pi/2n)} \tag{17}$$

It has been found that injecting the third harmonic leads to an increase of 15.47% in the fundamental output voltage while there is an increase of 5.12% by injecting the fifth harmonic [15], [20]. Following the same procedure, it can be derived that the injection of the nineth harmonic will lead to an increase of 1.54% in the fundamental output voltage.

2.2. Determination of the Common-node Zero-sequence Voltage with Balanced Load

Existence functions are modulation pulses having values of zero or unity. The Fourier series approximation of the existence functions are represented as follows [3], [13]:

$$
\begin{aligned}
S_{ap} &\cong 0.5(1 + M_{ap}) \\
S_{bp} &\cong 0.5(1 + M_{bp}) \\
S_{cp} &\cong 0.5(1 + M_{cp}) \\
S_{dp} &\cong 0.5(1 + M_{dp}) \\
S_{ep} &\cong 0.5(1 + M_{ep}) \\
S_{fp} &\cong 0.5(1 + M_{fp}) \\
S_{gp} &\cong 0.5(1 + M_{gp}) \\
S_{hp} &\cong 0.5(1 + M_{hp}) \\
S_{ip} &\cong 0.5(1 + M_{ip})
\end{aligned}
\tag{18}
$$

Where M_{ap}, M_{bp}, M_{cp}, M_{dp}, M_{ep}, M_{fp}, M_{gp}, M_{hp}, M_{ip} are the carrier-based modulation signals. Their values range between -1 and 1. For implementation, the existence functions are generated by comparing the high-frequency carrier signal (triangle signal) having positive peak and negative peak values of 1 and -1 respectively. The frequency of the carrier signal adopted for this work is 10kHz. After some simplifications that involve substituting (18) and (8) into (3), the modulation signals for the top nine switching devices can be expressed as:

$$
M_{jp} = \frac{2(v_{jn} + v_{no})}{v_{dc}} = \frac{2v_{jn}}{v_{dc}} + \frac{2v_{no}}{v_{dc}} = M_{jp}^* + M_o^* \tag{19}
$$
$$
j = a,b,c,d,e,f,g,h,i
$$

Where M_{jp}^* are the reference modulation signals for the phases, M_{jp} are the corresponding actual modulation signals responsible for generating the switching functions, M_o^* is responsible for producing the zero-sequence signal (common-node voltage) injection in the carrier-based PWM VSI. The modulations signals synthesized in (19) are compared with the carrier signal such that the respective switch turns on when the corresponding modulation signal is greater than the triangle carrier signal and vice versa. Furthermore, as the device turns on, the complimentary switch on the particular leg turns off owing to the Kirchhoff's Voltage Law constraint imposed on the existence function as mentioned earlier.

A properly selected zero-sequence signal can extend the linearity region of the carrier-based PWM VSI. From the earlier works on this subject [3], [13], the expression for generating the zero-sequence signal (common-node voltage) is:

$$v_{no} = 0.5v_{dc}(1 - 2\alpha) - \alpha v_{min} + (\alpha - 1)v_{max} \tag{20}$$

Where v_{min} and v_{max} represent the instantaneous minimum and maximum magnitudes of the nine reference modulating voltages as shown in (21). α can assume any value between zero and unity but $\alpha = 0.5$ is considered the best overall in every linear condition and it is the value chosen for this work. The value,

$\alpha = 0.5$, has also been found to give state vector PWM (SVPWM) scheme.

$$v_{\min} = \min \left[v_{an}^*, v_{bn}^*, v_{cn}^*, v_{dn}^*, v_{en}^*, v_{fn}^*, v_{gn}^*, v_{hn}^*, v_{in}^* \right]$$
$$v_{\max} = \max \left[v_{an}^*, v_{bn}^*, v_{cn}^*, v_{dn}^*, v_{en}^*, v_{fn}^*, v_{gn}^*, v_{hn}^*, v_{in}^* \right]$$
(21)

By dividing both sides of (20) by $0.5v_{dc}$, the expression for the average value of M_o^* is given as:

$$\frac{v_{no}}{0.5v_{dc}} = (1 - 2\alpha) - \alpha \frac{v_{\min}}{0.5v_{dc}} + (\alpha - 1) \frac{v_{\max}}{0.5v_{dc}}$$
$$\Rightarrow \langle M_o^* \rangle = (1 - 2\alpha) - \alpha M_{\min}^* + (\alpha - 1) M_{\max}^*$$
(22)

Where $M_{\min}^*$ and $M_{\max}^*$ are the instantaneous minimum and maximum magnitudes of the reference modulation signals for the nine phases.

Figure 2 is the schematic diagram representing the nine-phase carrier-based PWM voltage source inverter incorporating both the ninth harmonic zero-sequence and the common-node zero-sequence injection technique. A model corresponding to this schematic diagram was implemented using MATLAB/Simulink.

2.3. Determination of the Common-node Zero-sequence Voltage with Unbalanced Load

The common-node zero-sequence voltage signal for the nine-phase system will not be zero when the load is unbalanced since there will be a resultant current i_{js} in (1) as a result of the imbalance. Consequently, the procedure adopted to determine the common-node zero sequence signal will not be applicable here. Following the procedure adopted for five-phase system in [3], the system voltage equation shown in (3) will be re-arranged as follows:
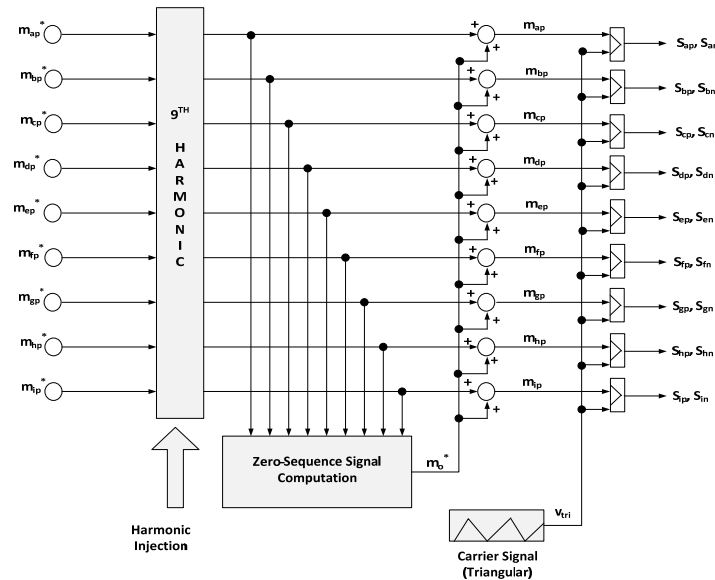
$$v_{jo} = v_{jn}^* + v_{no}^*$$
(23)

Figure 2. Nine-phase carrier-based PWM technique

In (23), the pole (switched) inverter voltage is expressed in terms of the reference inverter output voltage v_{jn}^*, and the average common-node neutral voltage v_{no}^*.

Equation (18) can be generically expressed as:

$$S_{jp} = 0.5(1 + M_{jp}), j = a,b,c,d,e,f,g,h,i \tag{24}$$

Substituting (24) into (8) gives:

$$v_{jo} = 0.5v_{dc}M_{jp} \tag{25}$$

Also, substituting (25) into (23) gives:

$$0.5v_{dc}M_{jp} = v_{jn}^* + v_{no}^* \tag{26}$$

Equation (26) can be re-arranged to give:

$$M_{jp} = \frac{v_{jn}^*}{0.5v_{dc}} + \frac{v_{no}^*}{0.5v_{dc}}$$
$$\Rightarrow M_{jp} = M_{jp}^* + M_o^* \tag{27}$$

Where,

$$M_{jp}^* = \frac{v_{jn}^*}{0.5v_{dc}}$$
$$M_o^* = \frac{v_{no}^*}{0.5v_{dc}} \tag{28}$$

From (27),

$$M_{jp} - M_o^* = M_{jp}^* \tag{29}$$

Equation (29) can be expressed in matrix form as follows:

$$\begin{bmatrix} 1 & 0 & 0 & 0 & 0 & 0 & 0 & 0 & 0 & -1 \\ 0 & 1 & 0 & 0 & 0 & 0 & 0 & 0 & 0 & -1 \\ 0 & 0 & 1 & 0 & 0 & 0 & 0 & 0 & 0 & -1 \\ 0 & 0 & 0 & 1 & 0 & 0 & 0 & 0 & 0 & -1 \\ 0 & 0 & 0 & 0 & 1 & 0 & 0 & 0 & 0 & -1 \\ 0 & 0 & 0 & 0 & 0 & 1 & 0 & 0 & 0 & -1 \\ 0 & 0 & 0 & 0 & 0 & 0 & 1 & 0 & 0 & -1 \\ 0 & 0 & 0 & 0 & 0 & 0 & 0 & 1 & 0 & -1 \\ 0 & 0 & 0 & 0 & 0 & 0 & 0 & 0 & 1 & -1 \end{bmatrix} \begin{bmatrix} M_{ap} \\ M_{bp} \\ M_{cp} \\ M_{dp} \\ M_{ep} \\ M_{fp} \\ M_{gp} \\ M_{hp} \\ M_{ip} \end{bmatrix} = \begin{bmatrix} M_{ap}^* \\ M_{bp}^* \\ M_{cp}^* \\ M_{dp}^* \\ M_{ep}^* \\ M_{fp}^* \\ M_{gp}^* \\ M_{hp}^* \\ M_{ip}^* \end{bmatrix} \tag{30}$$

Just like in [3], Equation (30) can be represented as follows:

$$Ax = y \tag{31}$$

Where,

$$A = \begin{bmatrix} 1 & 0 & 0 & 0 & 0 & 0 & 0 & 0 & 0 & -1 \\ 0 & 1 & 0 & 0 & 0 & 0 & 0 & 0 & 0 & -1 \\ 0 & 0 & 1 & 0 & 0 & 0 & 0 & 0 & 0 & -1 \\ 0 & 0 & 0 & 1 & 0 & 0 & 0 & 0 & 0 & -1 \\ 0 & 0 & 0 & 0 & 1 & 0 & 0 & 0 & 0 & -1 \\ 0 & 0 & 0 & 0 & 0 & 1 & 0 & 0 & 0 & -1 \\ 0 & 0 & 0 & 0 & 0 & 0 & 1 & 0 & 0 & -1 \\ 0 & 0 & 0 & 0 & 0 & 0 & 0 & 1 & 0 & -1 \\ 0 & 0 & 0 & 0 & 0 & 0 & 0 & 0 & 1 & -1 \end{bmatrix} \tag{32}$$

On closer look at (32), there are ten columns and nine rows. This implies that there are nine equations with ten unknown in (27). The solution to (31) is indeterminate and by invoking the Moore-Penrose pseudo-inverse method. The solution is obtained as:

$$x = A^T \left(A A^T \right)^{-1} y \tag{33}$$

Consequently, the modulation signals are obtained as:

$$M_{jp} = \frac{1}{10} \left(9 M^*_{jp} - \sum_{\substack{k=a \\ k \ne j}}^{i} M^*_{kp} \right) \tag{34}$$

By re-arranging (34), the common-node zero-sequence signal as a result of load imbalance is obtained as:

$$M^*_o = -\frac{1}{10} \sum_{k=a}^{i} M^*_{kp} \tag{35}$$

3.   RESULTS AND ANALYSIS

The model of a carrier-based PWM two level voltage source inverter for 9-phase induction machine drive was developed and simulated using MATLAB/Simulink. Detailed analysis encompassing the ninth harmonic zero-sequence injection and common-node zero-sequence signal injection was implemented. The analysis of the system under balanced and unbalanced load was also carried out. For this work, the frequency of the carrier signal (V_{tri}) used is 10kHz and the value of the dc bus voltage (V_{dc}) utilized was 150 V. The parameters for the nine-phase squirrel cage induction machine used as the system load are listed in Table 1.

The prototype machine used was a three-phase induction machine (with a rated peak voltage of 180 V) that was rewound to a nine phase machine. Consequently, the peak voltage for the nine phase machine is 60V.

Table 1. Parameters of the Nine-Phase Squirrel Cage Induction Machine

Parameter	value
Rated Power	3 Horsepower (hp)
Stator Resistance (R_s)	0.99 Ω
Referred Rotor Resistance (R'_r)	0.66 Ω
Magnetizing inductance (L_{ms})	0.0404 H
Stator Leakage Inductance (L_{ls})	0.0034 H
Referred Rotor Leakage Inductance (L'_{lr})	0.0034 H
Number of Poles	4
Moment of Inertia (J)	0.089 kg.m^2

3.1. PWM Algorithm for Balanced Modulation Signals and Balanced Load

Simulation results for the carrier-based PWM voltage source inverter in which the modulation signals for all the nine phases are balanced and the load is also balanced are presented here. The value, $\alpha = 0.5$, was chosen for the common-node zero-sequence voltage injection. The effect of this value of α on the modulation signal can be seen in Figure 3 part (b). Figure 4 part (a) shows the inverter output phase 'a' voltage while part (b) shows the load current when a load torque of 9 Nm was applied to the induction motor. Figure 5 shows the inverter output line-to-line voltage for adjacent phases (phase 'a' and phase 'b'), and nonadjacent phases (phase 'a' and phase 'c').

Figure 3. Phase 'a' modulation signal (a) Given reference modulation signal (b) actual modulation signal with $\alpha = 0.5$

In Figure 6, the electromagnetic torque and rotor speed characteristics of the induction machine are presented. It can be seen from the figures that the rated electromagnetic torque of the nine-phase squirrel cage induction machine is about 12Nm. Parts (a) and (b) respectively show the electromagnetic torque and rotor speed of the machine during free acceleration period while parts (c) and (d) show same after a 9Nm load torque is applied to the machine at 3 seconds. The nine-phase stator currents of the squirrel cage induction machine are shown in the plot of Figure 7.
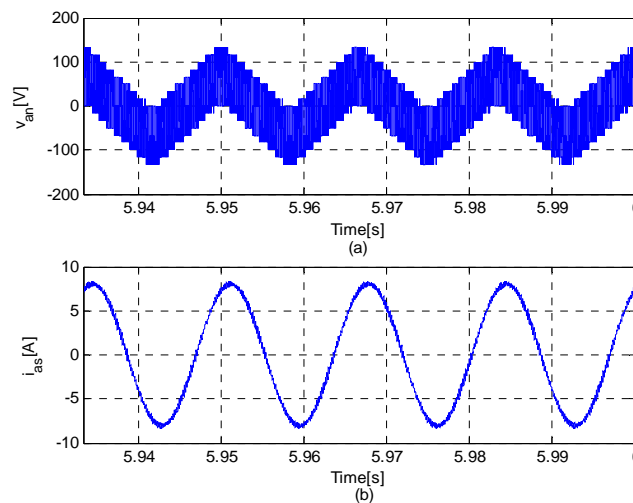
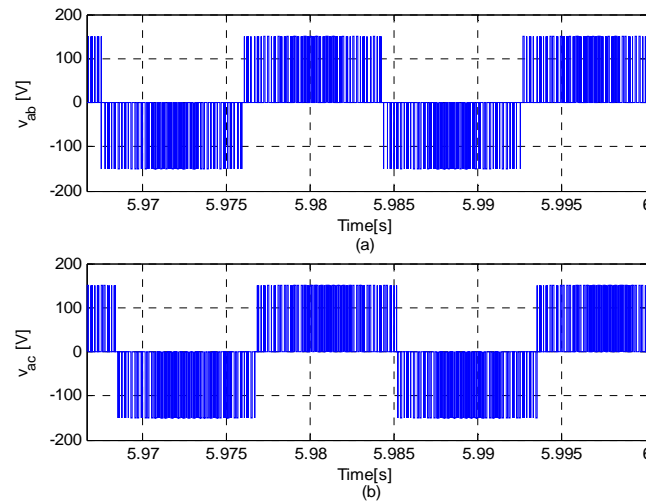Figure 4. (a) Phase 'a' load voltage (b) phase 'a' stator current

Figure 5. (a) Line-to-line voltage for phase 'a' and phase 'b' (b) line-to-line voltage for phase 'a' and phase 'c'

3.2. PWM Algorithm for Unbalanced Modulation Signals and Balanced Load

In this segment of simulation results analysis, the carrier-based PWM voltage source inverter has unbalanced modulation signals. However, it is made to supply a balanced load (symmetrical nine-phase induction machine). The imbalance was occasioned by interchanging the phase angles of the modulation signals (reference voltages) for phase 'a' and phase 'b'; also, the magnitude for phase 'd' modulation signal was changed from 0.8 to 0.78. This translated to the peak value of phase 'd' reference voltage changing from 60 V to 47 V. The common-node neutral voltage is generated through the procedure laid down in section 2 subsection 2.3 above.
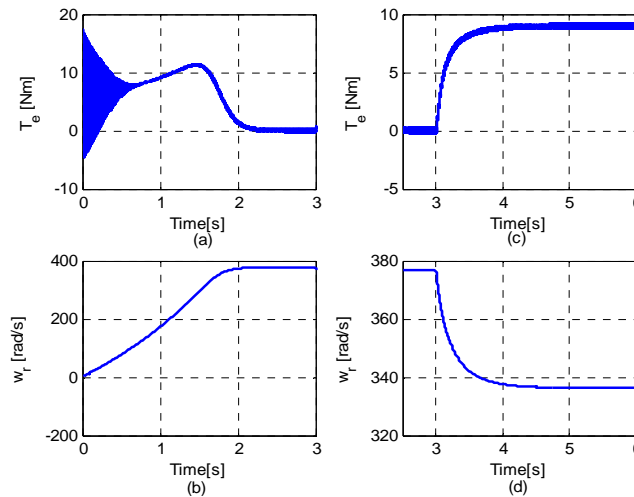

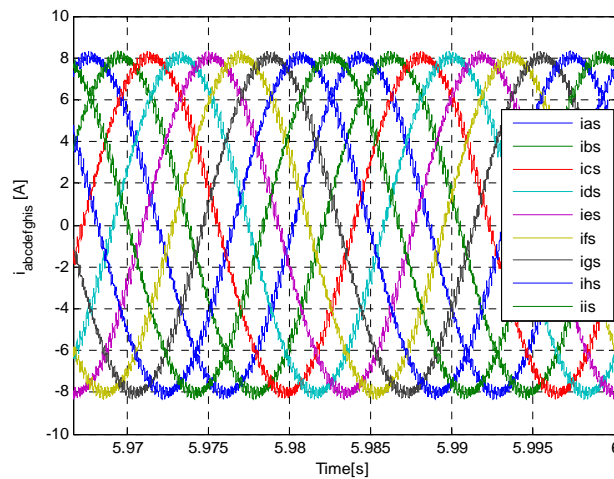Figure 6. Plots of electromagnetic torque and rotor speed

Figure 7. Nine-phase induction machine stator currents

Figure 8 part (a) shows the inverter output phase 'a' voltage while part (b) shows the load current when a load torque of 9 Nm was applied to the induction motor.
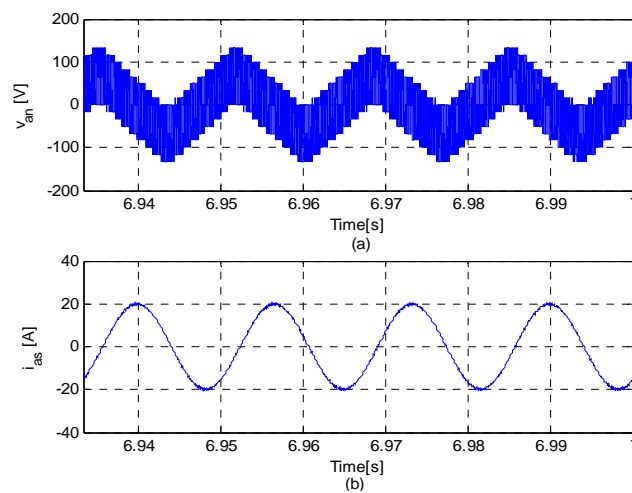

Figure 8. (a) Phase 'a' load voltage (b) phase 'a' stator current

In Figure 9, the electromagnetic torque and rotor speed characteristics of the induction machine are presented. Parts (a) and (b) respectively show the electromagnetic torque and rotor speed of the machine during free acceleration period while parts (c) and (d) show the same after a 9Nm load torque is applied to the machine at 3 seconds. Due to the imbalance in the modulation signals, the electromagnetic torque exhibits some oscillations and the rated value has decreased to about 10Nm. There is a larger slip in rotor speed on application of load torque as compared to the first (section 3.1) scenario

The complete nine-phase stator currents of the squirrel cage induction machine during this faulty inverter operating condition are shown in the plot of Figure 10. The magnitudes of the load currents flowing in the two phases (phase 'a' and phase 'b') with the wrong modulation signal phase angles can be seen to be larger than the rest.

3.3. PWM Algorithm for Balanced Modulation Signals and Unbalanced Load

In this final part of the analysis, the carrier-based PWM voltage source inverter has unbalanced modulation signals just like in section 3, subsection 3.2 above. However, unlike section 3.2, it is made to supply an unbalanced load (asymmetrical nine-phase induction machine). The imbalance in the load is caused by the loss of one phase in the stator winding (open-stator fault) of the machine. In this particular

case, phase 'a' of the stator windings was opened. The common-node neutral voltage is generated through the procedure laid down in section 2 subsection 2.3.
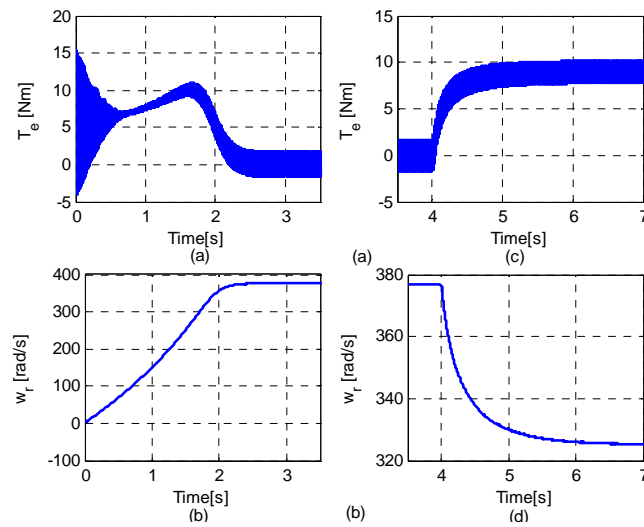

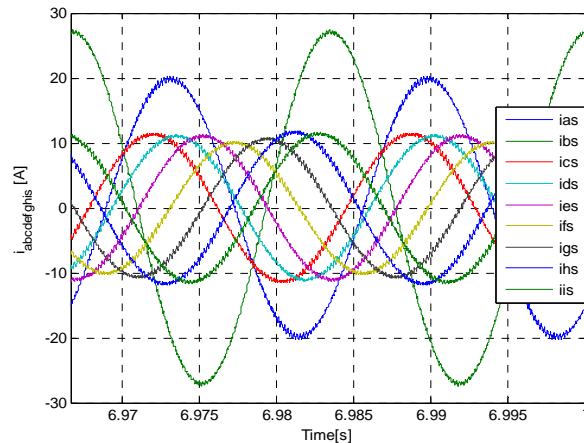Figure 9. Plots of electromagnetic torque and rotor speed

Figure 10. Nine-phase induction machine stator currents

In Figure 11, the electromagnetic torque and rotor speed characteristics of the induction machine under this asymmetrical operation are presented. Parts (a) and (b) respectively show the electromagnetic torque and rotor speed of the machine during free acceleration period while parts (c) and (d) show same after a 9Nm load torque is applied to the machine at 3 seconds. It can be see that the electromagnetic torque exhibits more oscillations as compared to those in Figure 9. The machine rated electromagnetic torque has further decreased to about 9 Nm. There is also a large slip in rotor slip experienced on application of load torque under this faulty condition. Slip is the difference between the synchronous speed and the rotor speed.

The effects of the imbalance in the inverter and the load can be seen on the complete nine-phase stator currents of the squirrel cage induction machine as shown in the plot of Figure 12. The magnitude of phase 'a' current is zero while the magnitude of phase 'b' current can be seen to be considerably higher than the rest.
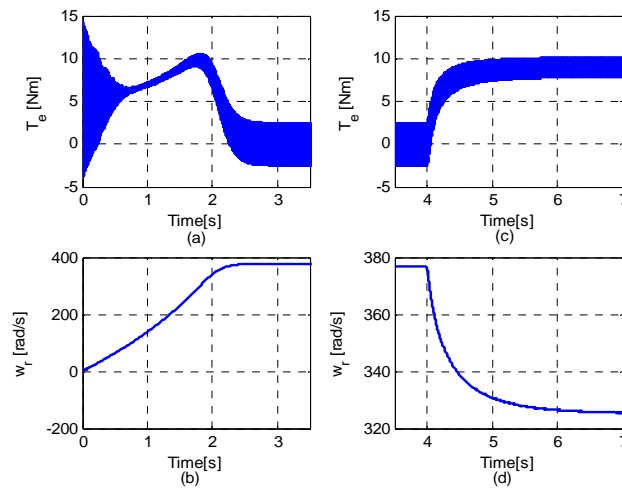
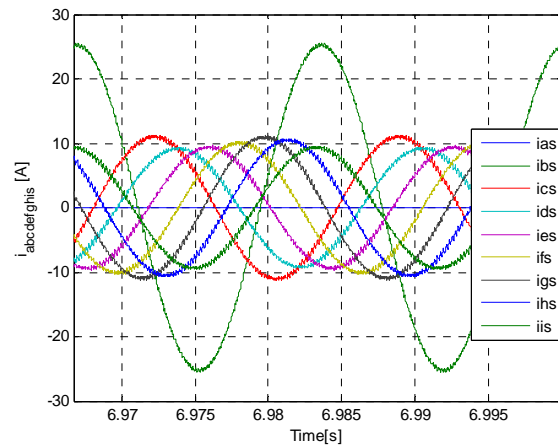Figure 11. Plots of electromagnetic torque and rotor speed

Figure 12. Nine-phase induction machine stator currents

4. CONCLUSION

In this paper, a carrier-based PWM two level voltage source inverter for nine phase induction machine drive was developed. Detailed equations for modeling the nine-phase VSI were clearly laid out and simulation results are presented. The effects of imbalance in the modulation signals of the carrier based VSI and imbalance on the induction machine load were investigated. The imbalance in the modulation signals of the VSI resulted in some oscillation of the electromagnetic torque of the machine with a relative drop in the torque rating. For the imbalance involving the modulation signals and the load, the oscillation of the electromagnetic torque were quite severe. Also, compared to the normal inverter and induction machine operation, there are substantial drops in rotor speed (slip) on application of load torque in the two imbalance scenarios considered.

REFERENCES

[1] Momoh OD. Nine-phase squirrel cage induction machine: Sustainable energy applications. Encyclopedia of Energy Engineering and Technology, Taylor and Francis. 2013.
[2] L Zarri, et al. *Behavior of multiphase induction machines with unbalanced stator windings.* Proc. International Symposium on Diagnostics for Electric Machines, Power Electronics & Drives (SDEMPED). 2011; 84-91
[3] S Karugaba, O Ojo. A carrier-based PWM modulation technique for balanced and unbalanced reference voltages in Multiphase voltage-source inverter. *IEEE Trans. Industry Application.* 2012; 48(6): 2102-2109.
[4] J Huang, et al. *Multiphase machine theory and its applications.* Proc. International Conference on Electrical Machines and Systems (ICEMS). 2008: 1-7.

[5]   H Tao, et al. Magnetostructural coupling field analysis on the end winding of a multiphase induction machine. *TELKOMNIKA Indonesian Journal of Electrical Engineering*. 2012; 10(5): 933-939.

[6]   A Gautam, O Ojo, M Ramzani, OD Momoh. *Computation of equivalent circuit parameters of nine-phase induction motor in different operating modes* Proc. IEEE Energy Conversion Congress and Exposition (ECCE). 2012: 142-149.

[7]   GK Singh. Multi-phase induction machine drive research – a survey. *Electric Power Systems Research*. 2002; 61: 139-147.

[8]   S Karugaba, G Wang, O Ojo, M Omoigui. *Dynamic and steady-state operation of a five phase induction machine with an open stator phase.* Proc. 40th IEEE North American Power Symposium NAPS '08. 2008: 1-8.

[9]   AA Rockhill, TA Lipo. *A simplified model of a nine phase synchronous machine using vector space decomposition.* Proc. IEEE Power Electronics and Machine in Wind Applications (PEMWA 2009). 2009: 1-5.

[10] S Brisset, D Vizireanu, P Brochet. Design and optimization of a nine-phase axial-flux PM synchronous generator with concentrated winding for direct-drive wind turbine. *IEEE Trans. Industry Application*. 2008; 44(3): 707-715.

[11] E Jung, et al. A nine-phase permanent magnet motor drive system for an ultrahigh-speed elevator. *IEEE Trans. Industry Application*. 2012; 48: 987-995.

[12] S Sadeghi, et al. Wide operational speed range of five-phase permanent magnet machines by using different stator winding configurations. *IEEE Trans. Industrial Electronics*. 2012; 59(6): 2621-2631.

[13] O Ojo. The generalized discontinuous PWM scheme for three-phase voltage source inverters. *IEEE Trans. Industrial Electronics*. 2004; 51(6): 1280-1289.

[14] SM Ahmed, et al. Carrier based Pulse Width Modulation Control of a NonSquare direct matrix converter with seven phase input and three phase output. *International Journal of Power Electronics and Drive Systems (IJPEDS)*. 2013; 3(3): 344-350.

[15] A Iqbal, S Moinuddin. Comprehensive relationship between carrier-based PWM and space vector PWM in a five-phase VSI. *IEEE Trans. Power Electronics*. 2009; 24(10): 2379-2390.

[16] V Blasko. Analysis of a hybrid PWM based on modified space-vector and triangle-comparison methods. *IEEE Trans. Industrial Electronics*. 1997; 33(3): 756-764.

[17] AM Hava, RJ Kerkman, TA Lipo. Simple analytical and graphical methods for carrier-based PWM-VSI drives. *IEEE Trans. Power Electronics*. 2009; 14(1): 49-61.

[18] KS Gowri, TB Reddy, CS Babu. *A novel high performance generalized discontinuous PWM algorithm for reduced current ripple and switching losses using imaginary switching times.* Proc. 2008 IEEE Region 10 Conference. 2008: 1-6.

[19] K Zhou, D Wang. Relationship between space-vector modulation and three-phase carrier-based PWM: A comprehensive analysis. *IEEE Trans. Industrial Electronics*. 2002; 49(1): 186-196.

[20] A Iqbal, et al. Generalized sinusoidal PWM with harmonic injection for multi-phase VSIs. *37th IEEE Power Electronics Specialists Conference (PESC'06)*. 2006: 1-7.

[21] D Dujic, et al. *Continuous PWM techniques for sinusoidal voltage generation with seven-phase voltage source inverters.* IEEE Power Electronics Specialists Conference (PESC'07). 2007: 47-52.